LANGMUIR

Article

pubs.acs.org/Langmuir

Examining Nanoparticle Adsorption on Electrostatically "Patchy" Glycopolymer Brushes Using Real-Time ζ-Potential Measurements

Ramya Kumar,[†,⊥] Irina Kopyeva,[†,⊥] Kenneth Cheng,[‡,⊥] Kai Liu,[†,⊥] and Joerg Lahann*[,†,‡,§,∥,⊥]

[†]Department of Chemical Engineering, [‡]Department of Material Science & Engineering, [§]Department of Macromolecular Science & Engineering, [∥]Department of Biomedical Engineering, and [⊥]Biointerfaces Institute, University of Michigan, Ann Arbor, Michigan 48109, United States

Supporting Information

ABSTRACT: Biomaterial surfaces can possess chemical, topographical, or electrostatic heterogeneity, which can profoundly influence their performance. By developing experimental models that reliably simulate this nanoscale heterogeneity, we can predict how heterogeneous surfaces are transformed by their interactions with the dynamic physiological environment. In this work, we present a model surface where well-defined glycopolymer brushes are interspersed with positively charged binding sites, giving rise to an interface presenting a mixture of repulsive and adhesive cues to an approaching virus particle. We show that the density of the affinity sites relative to the glycopolymer brushes can be tuned precisely by modifying the chemical vapor deposition (CVD) copolymerization conditions. Further, we examined the effects of binding site density and glycopolymer brush architecture on the adsorption kinetics of virus-like nanoparticles through a novel approach employing time-resolved ζ-potential measurements. Most materials have charge-bearing, dynamic surfaces that are sensitive to electrostatic effects. Hence, adsorption-triggered changes in ζ-potential measurements can be captured in real time to monitor interfacial events. Real-time ζ-potential measurements present an interesting platform to probe the structure and function of chemically and electrostatically heterogeneous polymer interfaces. To validate this electrokinetic method, we examined the effect of neutravidin concentration on its rate of binding to biotinylated surfaces using ζ-potential and compared our results with QCM studies. By applying electrokinetic methods to examine the roles of glycopolymer brush architecture and surface charge of these tunable glycopolymer coatings, we can enhance our understanding of the interactions of viruses with heterogeneous biomaterial interfaces.

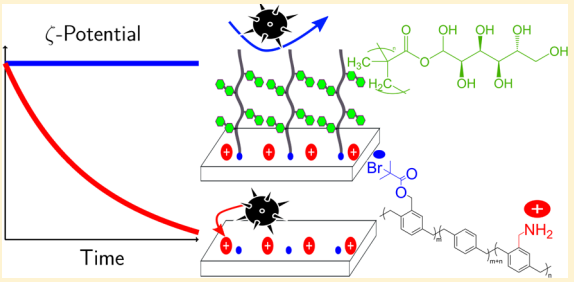

INTRODUCTION

Reliable experimental models can identify design specifications for optimal biomaterial performance, but developing a suitable model system is challenging. This is largely due to the complexity of biological responses triggered by the biomaterial within the host organism.[1] Interactions between biomaterials and the physiological environment, such as the formation and remodeling of the protein corona, or the receptor-mediated binding of viruses and cells,[2] begin within nanoseconds, but its effects can last for years.[3] In addition to dealing with the complex physiological environment, we have to take into account the additional layer of complexity inherent within heterogeneous biomaterial surfaces. Nanoscale heterogeneity can exist in several forms—the surface can contain randomly distributed domains of neutral, positive, and negative surfaces charge, or the surface could be amphiphilic with both hydrophobic and hydrophilic characteristics, leading to interesting interfacial behavior.[4] Consider the example of nonfouling polymer brushes that prevent nonspecific adsorption. Despite advances in surface-initiated polymerization techniques, it is possible for nanoscale defects to form in the brush due to trace impurities, low grafting density, or processing limitations.[5] As a result, the nonfouling performance of the brushes in a biomedical setting will be compromised,[6] leading to undesirable outcomes such as hospital-acquired infections and thrombosis.[7] Since the defects can interact with proteins and pathogen species through hydrogen bonding, van der Waals interactions, electrostatic attraction, or hydrophobic interactions, the surface simultaneously offers both adhesive and repulsive cues to the adsorbate species. A suitable experimental model will help us understand the adsorption characteristics of these chemically and topographically heterogeneous interfaces. The use of such model surfaces will ensure that interfacial interactions promote intended functional outcomes, ranging from the prevention of nonspecific adsorption to the modulation of bioactive molecules.

Santore and co-workers showed that electrostatically heterogeneous model surfaces possessing systematically engineered "defects" are useful in several contexts: the prevention of nonspecific adsorption, selective protein and bacterial capture, protein separation, and, importantly, fundamental understanding

Received: May 8, 2017
Revised: June 2, 2017
Published: June 2, 2017

DOI: 10.1021/acs.langmuir.7b01553
Langmuir XXXX, XXX, XXX−XXX

of the underlying mechanisms of adhesion.[8] By carefully introducing charged binding sites at the base of protein-resistant brushes, the competing effects of steric repulsion and electrostatic attraction could be controlled precisely, achieving the desired bioadhesion outcome.[9] Nanotextured surfaces composed of positively charged patches such as poly-L-lysine hydrobromide (PLL) and poly(ethylene glycol) (PEG) brushes have been used extensively as model systems to probe the effects of defect density, brush architecture, ionic strength, flow conditions, and protein and particle characteristics on the adsorption kinetics.[10−12] Though several useful insights have been gleaned from these surfaces, they have a few drawbacks. First, the creation of cationic patches and PEG brushes is based on physisorption rather than covalent attachment, imperiling their use in biological environments for long durations.[13] Second, even though PEG is the most commonly employed nonfouling polymer due to ease of synthesis, its use is fraught with the risk of auto-oxidative[14] degradation *in vivo*. Investigators seeking to identify alternatives possessing comparable nonfouling properties have concluded that zwitterionic polymer brushes and carbohydrate-based polymer brushes are promising options.[15] In a comparison of mannitol-terminated and PEG-terminated SAMs, it was discovered that PEG-terminated SAMs lost the fidelity of their cell patterns.[16] In contrast, mannitol patterns were able to retain their nonfouling properties over a long-term, and the cell pattern fidelity was preserved. From the perspective of technological relevance and clinical translation, it would be advantageous to replace PEG-based model systems with biomimetic carbohydrate-based model surfaces, while investigating the role of binding site density on the adsorption of proteins, bacteria, or viruses.

Carbohydrate-based polymer films are inspired by the sugary sheath surrounding the endothelial cells, the glycocalyx.[17] On account of its hydration and steric resistance, the endothelial glycocalyx can achieve near zero levels of nonspecific protein adsorption.[18] Theoretical and experimental studies indicate that glycocalyx-inspired surfaces composed of sorbitol and mannitol interact strongly with hydrating water molecules. These studies concluded that the enthalpic cost of disrupting this hydration layer generates repulsive forces and ultimately renders adsorption thermodynamically unfavorable.[19,20]

Through surface-initiated atom transfer radical polymerization (SI-ATRP) and chemical vapor deposition (CVD) copolymerization, we have developed a robust and substrate-independent glycopolymer brush platform. The versatility and control afforded by SI-ATRP enable us to create high spatial density of sorbitol molecules with any desired brush architecture. In addition, we have rendered the glycopolymer coating electrostatically heterogeneous by embedding positively charged binding sites or defects in the form of aminomethyl functional groups, which can be copresented with the sorbitol brushes in any desired ratio. In this paper, we describe the design and synthesis of a tunable electrostatically patchy glycopolymer brush interface that can build on the progress made by preceding model systems in understanding adhesion events. Additionally, we have demonstrated tunable binding of virus-like nanoparticles to our model surface by varying the relative densities of binding sites and glycopolymer brushes. We used carboxylate-functionalized polystyrene nanoparticles as "model viruses" for two reasons: (1) Its size is comparable to those of many viruses. (2) Most viruses have isoelectric points below 6, implying that they possess negative charge at physiological pH.[21]

To study adsorption kinetics at the nanometer scale, a variety of techniques have been used: attenuated total reflectance infrared spectroscopy[22,23] (ATR-IR), ellipsometry,[24] optical waveguide light mode spectroscopy[25,26] (OWLS), total internal reflection fluorescence[27,28] (TIRF), atomic force microscopy[29] (AFM), and quartz crystal microbalance dissipation[30,31] (QCM-D). In recent years, surface plasmon resonance spectroscopy[32,33] (SPR) has emerged as the gold standard for studying biointerfacial phenomena. The use of optical methods to track the binding of viruses and their nanoparticle surrogates is difficult owing to their small size and limited ability to scatter light.[34] Fluorescence-based schemes for viral detection are hindered by photobleaching and low emission rates. Hence, measuring the adsorption kinetics of virus-like particles to our surface would require alternative approaches. Since we are interested in visualizing binding events occurring on electrostatically heterogeneous surfaces, we decided to depart from the traditionally used toolbox listed above and, instead, explore an electrokinetic approach for the detection and time-resolved measurement of nanoparticle binding. In this work, we apply real-time ζ-potential measurements to study the adhesion of virus-like nanoparticles onto glycopolymer coatings.

Typically, biomaterials perform their function in an aqueous environment, where functional groups on its surface can be ionized, preferential adsorb ions, and eventually acquire an electrical double layer. Consequently, the ζ-potential is a sensitive indicator of interfacial charge development in physiological fluids such as blood.[35] Prior work has linked changes in the ζ-potential to biofilm formation,[36] viral adhesion,[37] changes in the performance of an implanted neuronal electrode,[38] progression of osteogenesis,[39] or the inflammatory response to a biomaterial.[40] Although electrostatic effects exert a profound influence over the rate at which biomolecules, pathogens, and cells adsorb to the material surface, there have been very few studies employing ζ-potential measurements to elucidate adsorption events in a time-resolved manner. In pioneering work, Norde et al.[41] reported that measuring temporal changes in ζ-potential was an effective way to record the adsorption kinetics of a charged protein, such as lysosyme, on a complementarily charged surface, such as glass or silica.[42] Here, the change of the ζ-potential from its baseline value was linearly dependent on the amount of adsorbed protein. Etheve and Dejardin[43] were able to build on this earlier work by simultaneously acquiring the values of both ζ-potential and the deposited mass of protein. The outcome was a defined relationship between the change in ζ-potential and the total amount of adsorbed protein. So far, in situ ζ-potential measurements have been predominantly used to characterize equilibrium states of surfaces exposed to proteins,[44,45] viruses,[46,47] or nanoparticles.[48,49] In comparison, time-resolved ζ-potential measurements are still in their infancy[50] in spite of their prominent potential for understanding interfacial events at a biomaterials interface in a label-free and inexpensive manner.

In this report, we examine the effect of the surface composition of electrostatically heterogeneous glycopolymer on the binding kinetics of virus-like nanoparticles using real-time ζ-potential measurements. Before we embarked on these measurements, we validated our electrokinetic approach by comparing its adsorption response with that of QCM. For this validation study, we chose to measure the adsorption kinetics of a well-characterized binding pair: neutravidin and biotin. This contribution employs electrokinetic measurements to study two interfacial processes: (i) the specific binding of neutravidin

DOI: 10.1021/acs.langmuir.7b01553
Langmuir XXXX, XXX, XXX−XXX

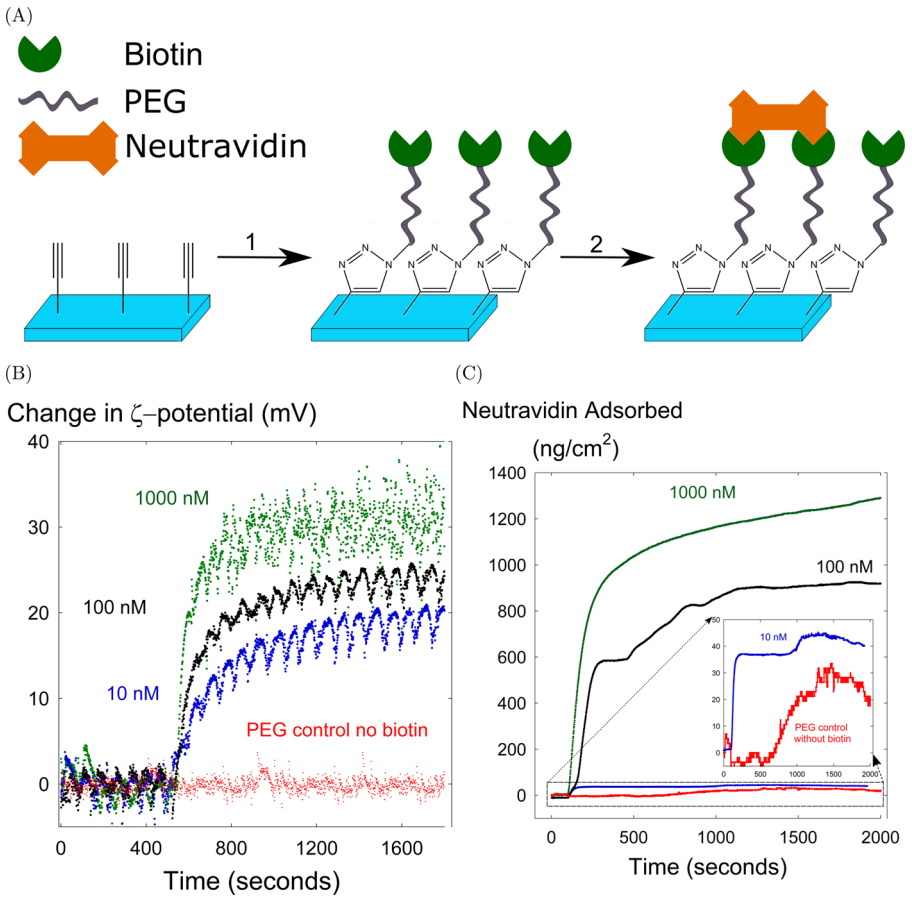

Figure 1. (A) In step 1, biotin-PEG-azide is conjugated to reactive alkyne groups on the PPX-alkyne substrate using Huisgen 1,3-dipolar cycloaddition. In step 2, neutravidin binds to the biotinylated surfaces. Binding kinetics were studied as a function of neutravidin concentration using (B) real-time ζ-potential measurements and (C) quartz crystal microbalance (QCM) measurements. Three concentrations of neutravidin were employed (10 nM in blue, 100 nM in black, and 1000 nM in green). For the control experiment, a PEGylated surface without any biotin was studied using a neutravidin concentration of 1000 nM (red). In both QCM and real-time ζ-potential measurements, the rate and extent of neutravidin adsorption were controlled by its solution concentration. Also, no adsorption could be detected in the control experiment even when the highest neutravidin concentration was employed.

to biotin with the objective of comparing adsorption trends with those from QCM and validating the technique; (ii) the nonspecific charge-promoted binding of virus-like nanoparticles to glycopolymer brush interfaces interspersed with positively charged binding sites.

RESULTS AND DISCUSSION

Binding Kinetics of Neutravidin to Biotinylated Surfaces Assessed via QCM and Real-Time ζ-Potential Measurements. Before conducting electrokinetic measurements to examine the adsorption of nanoparticles to electrostatically heterogeneous glycopolymer surfaces, we needed to establish the validity of this technique. We employed QCM studies in parallel with real-time ζ-potential measurements to investigate a well-established binding process and then compared results obtained from both methods. We wished to verify whether similar trends in neutravidin–biotin association are observed from both methods while monitoring the binding events in real time.

The noncovalent interaction between biotin and avidin analogues has been widely exploited in developing biosensors, drug delivery systems, biomolecular imaging probes, immunoassays, and other applications where high affinity and specificity are desired.[51] This is a well-established model for affinity interactions and is considered to be a reliable binding pair. Since biotin–avidin association happens extremely rapidly, the acquisition of kinetic data and determination of the binding constant for this interaction are quite challenging.[52] Nevertheless, the binding kinetics of streptavidin with biotin[53] has been thoroughly characterized by a variety of techniques, including fluorescence resonance energy transfer[52] (FRET), QCM-D,[54] and SPR.[55] Compared to streptavidin (pI of 5–6[56]) and avidin (pI of 10.5[56]), neutravidin (pI of 6.3[56]) has an isoelectric point closest to neutral pH and is expected to exhibit the least nonspecific binding among the three. Hence, neutravidin has been used in our study. We evaluate the adsorption kinetics of neutravidin on biotinylated surfaces using two methods in parallel: real-time ζ-potential measurements and QCM measurements.

The surfaces of the QCM crystals and the measurement surfaces of the electrokinetic analyzer were coated with poly(4-ethynyl-*p*-xylylene-*co*-*p*-xylylene) (PPX-alkyne), which displays highly reactive alkyne functional groups. The Huisgen 1,3-dipolar cycloaddition between azides and terminal alkynes was used to conjugate biotin-PEG-azide to the substrates using a procedure described in the Experimental Section and in previous reports.[57] To confirm that biotinylation was successful, fluorescence measurements were performed with both biotiny-

DOI: 10.1021/acs.langmuir.7b01553
Langmuir XXXX, XXX, XXX–XXX

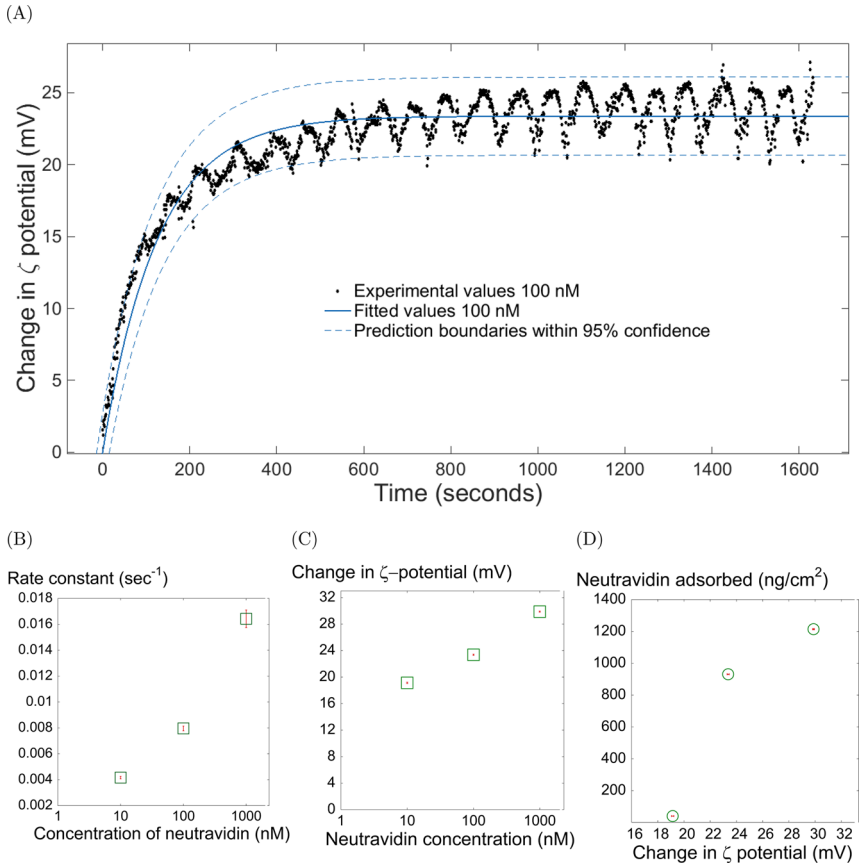

Figure 2. (A) Experimental values from the real-time ζ-potential measurements of the adsorption of 100 nM neutravidin to biotinylated surfaces were fitted to the monoexponential model with model parameters $A = 23.4$ mV and $k = 7.96 \times 10^{-3}$ s^{-1}. The model values (solid blue line) compare well with experimental values (black dots) within the prediction boundaries (95% confidence interval). The monoexponential model successfully captures the experimental adsorption trends despite the oscillations and scatter inherent to the technique. (B) Apparent rate constants are plotted against the logarithm of neutravidin concentration. The rate of neutravidin adsorption increases exponentially with concentration. (C) The magnitude of ζ-potential increase is plotted as a function of neutravidin concentration. (D) Calibration curve for ζ-potential change against the mass of bound neutravidin measured using QCM. Vertical and horizontal error bars are in red.

lated coverslips and non-biotinylated PEG-coated coverslips (negative control) using a fluorescently labeled streptavidin molecule. Fluorescence results are discussed in the Supporting Information.

After verifying that biotinylation was successful, we proceeded to detect and quantify the binding of neutravidin molecules to these surfaces (Figure 1A) using real-time ζ-potential measurements and QCM. In a typical measurement, the buffer was pumped through the measurement chamber, which was a flow cell in the form of a rectangular slit. Flow conditions in our measurement chamber are in the laminar regime, and the velocity profile can be described by the Hagen−Poiseuille equation. Since rapid transport of neutravidin is not possible in this flow setup, the rate constants observed from these studies are only transport-limited "apparent rate constants" and not the true rate constants.

The ζ-potential values were recorded continuously at a frequency of one measurement per second. After a stable baseline was established, neutravidin was injected into the flow circuit, and changes in ζ-potential could be observed in real time. Three concentrations of neutravidin were studied: 10, 100, and 1000 nM. In addition, a control experiment was performed at 1000 nM on a PEGylated surface devoid of biotin molecules. The adsorption response (Figure 1B) could be obtained by subtracting the average of the ζ-potential values collected during the baseline phase from the ζ-potential values obtained after the introduction of neutravidin. The average ζ-potential values collected during the baseline phase were quite similar across all experimental runs: −44 mV for the 10 nM experiment, −42.4 mV for the 100 nM experiment, and −41.93 mV for the 1000 nM experiment. In all three experiments, upon addition of neutravidin, the ζ-potential became less negative. However, the magnitude of increase in the ζ-potential was highest for the 1000 nM concentration at 29.9 mV, followed by the 100 nM run which had a 23.4 mV change (Figure 2C). Among the three experiments, the least change in ζ-potential (19.1 mV) was observed for the 10 nM experiment (Figure 2C). This change in ζ-potential can be attributed to the adsorption of neutravidin to the surface caused by its specific association with biotin molecules. It appears that the rate of increase of ζ-potential values as well as the magnitude of its increase is a function of neutravidin concentration, with higher concentrations promoting more rapid changes. When we consider the control experiment, the average baseline ζ-potential was −40.6 mV, which was only slightly higher than the values obtained with the biotinylated surfaces. However, when we added neutravidin to achieve a 1000 nM concentration, we did not observe any departure of the ζ-potential trends from baseline levels, indicating that neutravidin did not adsorb to the surface in the absence of biotin (Figure 1B).

DOI: 10.1021/acs.langmuir.7b01553
Langmuir XXXX, XXX, XXX−XXX

In our experiments, a target pressure of 150 mbar was employed to pump the fluid through the measurement chamber, and this pressure difference is achieved by the motorized movement of plungers placed within two 100 mL glass syringes. The oscillatory nature of the adsorption traces can be attributed to the periodic emptying and refilling of the syringe. Every time 100 mL of the electrolyte solution flows through the measurement chamber, this periodic refilling is performed to re-establish the target pressure. This cyclical pressure variation occurs every 90 s and is a typical feature of this technique. Further, overshoots in the target pressure can result in the spikes in the data. This scatter in the adsorption response has been observed in prior reports on time-resolved ζ-potential measurements.[43,50] When we constructed monoexponential adsorption models from the ζ-potential data (described in the next section), we concluded that this scatter does not affect the ability of the technique to clearly discriminate between adsorption trends from different neutravidin concentrations.

Next, we repeated this study using QCM instead of the ζ-potential (Figure 1C). In all three experiments performed with biotinylated surfaces (10, 100, and 1000 nM), we observed a decrease in frequency upon neutravidin addition. The frequency decrease was transformed into an estimate of adsorbed mass using the Sauerberey equation.[58] Neutravidin adsorption was highest when the concentration of neutravidin was 1000 nM, and an adsorption plateau of 1214 ng/cm^2 was reached. This plateau value was lowered dramatically when concentrations of 100 nM (931 ng/cm^2) and 10 nM (40.3 ng/cm^2) were used, indicating that the extent of neutravidin coverage on the surface is controlled by its concentration. This result mirrors what we observed in the ζ-potential studies performed using the same coatings and identical concentration values.

Interestingly, for the control experiment where the adsorption of 1000 nM neutravidin was measured on a PEGylated surface, a plateau value of 20−30 ng/cm^2 was obtained, which is only slightly less than the value (40.3 ng/cm^2) for the 10 nM experiment performed with a biotinylated surface (Figure 1C). Though a near-zero adsorption signal was obtained from this control surface using ζ-potential measurements in the 1000 nM neutravidin run, the adsorption signal from the parallel QCM control experiment is somewhat high. This suggests that the uptake of water and sodium phosphate salts by the QCM crystal also contributes to the adsorption signal. In the absence of measurements of the energy dissipation factor ΔD, it is difficult to subtract these non-neutravidin contributions from the buffer solution itself and obtain more accurate adsorption profiles. Results from our quantitative analysis are discussed in the next section.

Kinetic Modeling of Adsorption Data. Consistent with previous studies that employ Langmuirian adsorption kinetics, we assumed that neutravidin binding follows a first-order process and that our ζ-potential and QCM data can be described by a monoexponential fit. The model equation and fitting procedures are described in the Experimental Section. Two model parameters—(1) A, the plateau value of adsorption (units of mV for streaming potential and ng/cm^2 for QCM), and (2) k, the apparent rate constant of adsorption (units of s^{-1})—were computed within a 95% confidence interval. As an example, Figure 2A shows how closely the model (A = 23.4 mV and k = 7.96 × 10^{-3} s^{-1}) fits the experimental values for the ζ-potential experiment describing the kinetics of neutravidin adsorption at 100 nM. Despite the scatter in the data, we can see that most values fall within the prediction boundaries within a 95% confidence interval, indicating that the monoexponential model describes experimental behavior accurately. Five additional plots for the remaining experiments can be found in the Supporting Information (Figures S3 and S4) where the adsorption data from all ζ-potential and QCM experiments have been mapped. The model parameters and their uncertainties are tabulated in Tables S2 and S3 for ζ-potential and QCM, respectively. Model diagnostic tests were performed to evaluate the quality of our fitting, and these results are tabulated in Tables S4 and S5 for ζ-potential and QCM, respectively. We concluded that the monoexponential model matches our experimental trends for both measurement approaches.

From a closer look at the QCM adsorption traces, it appears that the biexponential model may have been more suitable than the monoexponential model. If we consider the QCM experiments performed at 10 nM and 100 nM, we can discern two phases of adsorption: an extremely rapid first phase and a slower second phase. After the initial exponential increase in adsorbed neutravidin is completed and a stable plateau value is attained, a second slower phase of adsorption begins. In contrast to the other two experiments, we do not detect two plateaus in the 1000 nM QCM run. Yet, we can see that the steep exponential climb is followed by a gradual linear growth in the mass of adsorbed neutravidin. This biphasic adsorption behavior can be explained by the heterogeneity of binding sites on the neutravidin molecule, with each site possessing different affinities.[52] Though the binding of the first biotin molecule is sterically unhindered and quite rapid, the binding of the second biotin molecule is hindered by the presence of adjacent biotin molecules that have already associated with neutravidin.[59] This two-step adsorption behavior was not evident in the ζ-potential experiments because electrokinetic methods, unlike QCM, lack the ability to detect changes in molecular orientation. Since this biphasic adsorption did not appear in the ζ-potential runs, we have used the monophasic monoexponential model for both the QCM and ζ-potential adsorption data for the sake of consistency and ease of modeling. From the model diagnostic tests, we concluded that the accuracy with which the monoexponential model predicts the QCM adsorption response is adequate.

In Figure 2B, we can see that the apparent rate constant of binding increases linearly with the logarithm of neutravidin concentration, a result which is in good agreement with previous studies. The apparent binding constant extracted from the slope of this plot is in the order of 10^4 M^{-1} s^{-1}, which is far lower than values of 3.0 × 10^6−4.5 × 10^7 M^{-1} s^{-1} reported using droplet microfluidics techniques,[52,60] where the transport limitation is greatly minimized by rapid mixing. In comparison, ζ-potential measurement is quite limited in its ability to characterize rapid binding processes, resulting in an apparent neutravidin−bioitin binding constant that is 2−3 orders of magnitude lower.

We can define a binding constant in terms of the adsorption response by evaluating the slope of Figure 2C (9.4 mV/μmol of neutravidin), which allows us to estimate the neutravidin concentration from the change in ζ-potential. In addition, we have mapped the adsorption signal from real-time ζ-potential measurements to the values of adsorbed neutravidin mass from QCM (Figure 2D), providing a means to evaluate the quantity of bound neutravidin from the ζ-potential signal.

We conducted a parallel study of neutravidin−biotin adsorption in order to compare results from from QCM and real-time ζ-potential measurements. We concluded that time-resolved electrokinetic measurements can yield kinetic trends that closely mirror those obtained from QCM. Upon completion

DOI: 10.1021/acs.langmuir.7b01553
Langmuir XXXX, XXX, XXX−XXX

of the investigation of biotinylated surfaces, we proceeded to interrogate electrostatically heterogeneous glycopolymer surfaces using this validated technique.

Tuning the Surface Density of Binding Sites on Brush Surfaces. Next, we applied real-time ζ-potential measurements to evaluate the adsorption kinetics of nanoparticulate models of viruses[34] on electrostatically heterogeneous polymer brush surfaces. Our surface design seeks to recapitulate aspects of the nanostructured organization of brush-like interfaces found in the body, most particularly the endothelial glycocalyx.[61] Our composite surface consists of two components (Figure 3A).

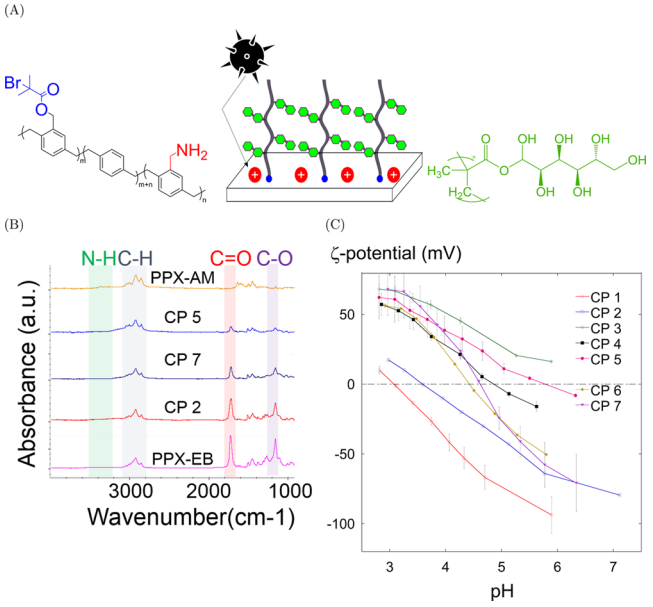

Figure 3. (A) Surface design used in our study. The base layer is composed of a copolymer synthesized using chemical vapor deposition, incorporating binding sites (aminomethyl groups or AM), and polymerization initiation sites (ester bromide or EB). Negatively charged nanoparticles were expected to attach to the AM groups, and we studied nanoparticle adsorption kinetics for different copolymer compositions. Sorbitol methacrylate brushes were grafted from the EB sites through SI-ATRP. (B) FTIR spectra showed that ratio of AM and EB is tunable. The decrease in peak heights of the carbonyl peak around 1730 cm^{-1} indicated that the ratio of EB relative to AM was reduced. (C) Surface charge of copolymer surfaces became more positive with increasing AM concentration. The isoelectric point was varied from 3 to 6 by changing the copolymer composition. Seven copolymer surfaces were studied (CP1 through CP7).

The first element is a copolymer formed by chemical vapor deposition (CVD) copolymerization of two paracyclophane-based monomers. One comonomer contains an initiator (ester bromide or EB) for surface-initiated atom transfer radical polymerization (SI-ATRP) and the other comonomer an ionizable amine moiety (aminomethyl or AM). The protonated amine functions as a positively charged binding site to which negatively charged species of interest such as viruses[21] can adsorb. The second element is composed of glycopolymer brushes bearing sorbitol side chains, which are grafted from the EB initiation sites on the copolymer using SI-ATRP. The density of the binding sites relative to that of the SI-ATRP initiation sites on the copolymer coating can be tuned by modifying the CVD copolymerization conditions. The model system can provide answers to the following questions: How does the density of aminomethyl groups affect the rate of adsorption of the virus-like nanoparticles? How does the introduction of a glycopolymer brush influence the adsorption behavior?

First, the surface composition of the copolymer was tuned by varying the CVD process parameters as described in the Experimental Section. To engineer varying ratios of AM and EB functional groups, copolymers were prepared using different CVD parameters. As seen in Figure 3B, the FTIR spectra show an increasing intensity of the carbonyl peak of the EB component from top to bottom, indicating that the surface concentration of the AM group in the copolymer was reduced successively. We concluded that surface composition is tunable and that the ratios of ester bromide and aminomethyl functional groups present on the surface could be controlled merely by varying the CVD parameters appropriately.

To further validate this result, we employed ζ-potential measurements to compare the interfacial charge of these copolymers of varying surface compositions. It was hypothesized that if a greater number of aminomethyl groups were present on the surface, then the resulting copolymer would carry a higher positive charge than a copolymer containing fewer aminomethyl groups. Figure 3C summarizes the results of this study wherein the ζ-potential values of the seven copolymer coatings (CP1 through CP7) are plotted as a function of pH. The copolymer surfaces had isoelectric points (IEPs) ranging from 3 to 6, where the copolymer surfaces with IEPs close to 3 were mostly composed of the ester bromide whereas those closer to 6 were dominated by the aminomethyl containing repeating unit. We concluded that our copolymer charge could be tuned by controlling surface composition and that a progressively more positively charged surface could be obtained by increasing the concentration of aminomethyl groups relative to the ester bromide groups.

Adsorption Rate of PS-COOH Nanoparticles Can Be Tuned by Varying the Surface Composition. We studied three surfaces of varying AM/EB ratios and isoelectric points of 5.7, 4.8, and 3.6. The pH was maintained constant at 6.0 for all experiments. Though this pH value is higher than the isoelectric points of all three copolymers, we anticipated that the proportion of ionized amine groups would be highest on the copolymer with the isoelectric point of 5.7.

We continuously measured changes in ζ-potential values with time before and after the addition of the nanoparticles. The addition of the PS-COOH nanoparticles to the electrolyte solution was accompanied by a steady decrease in the ζ-potential for all three samples (Figure 4). However, for copolymers with IEPs of 5.7 and 4.8, the decrease of ζ-potential was faster than it was for the sample with an IEP of 3.6. This is consistent with the predictions of models describing electrostatically driven adsorption,[62] which demonstrate that a greater availability of binding sites increases the rate constant for the adsorption step. Also, the magnitude of ζ-potential change (160 and 122 mV) was higher for the amine-rich surfaces than for the surfaces on which the EB groups were more abundant (51 mV). The relationship between adsorption rates and copolymer composition could be clearly discerned using real-time ζ-potential measurements. We concluded that nanoparticle adsorption rates could be tuned by modifying the surface concentration of aminomethyl groups.

Next, we studied the effect of incorporating glycopolymer brushes on the adsorption rate of nanoparticles. Poly(sorbitol methacrylate) brushes were grafted from the three sets of copolymers prepared. In all three cases, the adsorption rate was dramatically lower than what was observed without the polymer brushes. In two of the three experiments (Figure 4B,C), the

DOI: 10.1021/acs.langmuir.7b01553
Langmuir XXXX, XXX, XXX−XXX

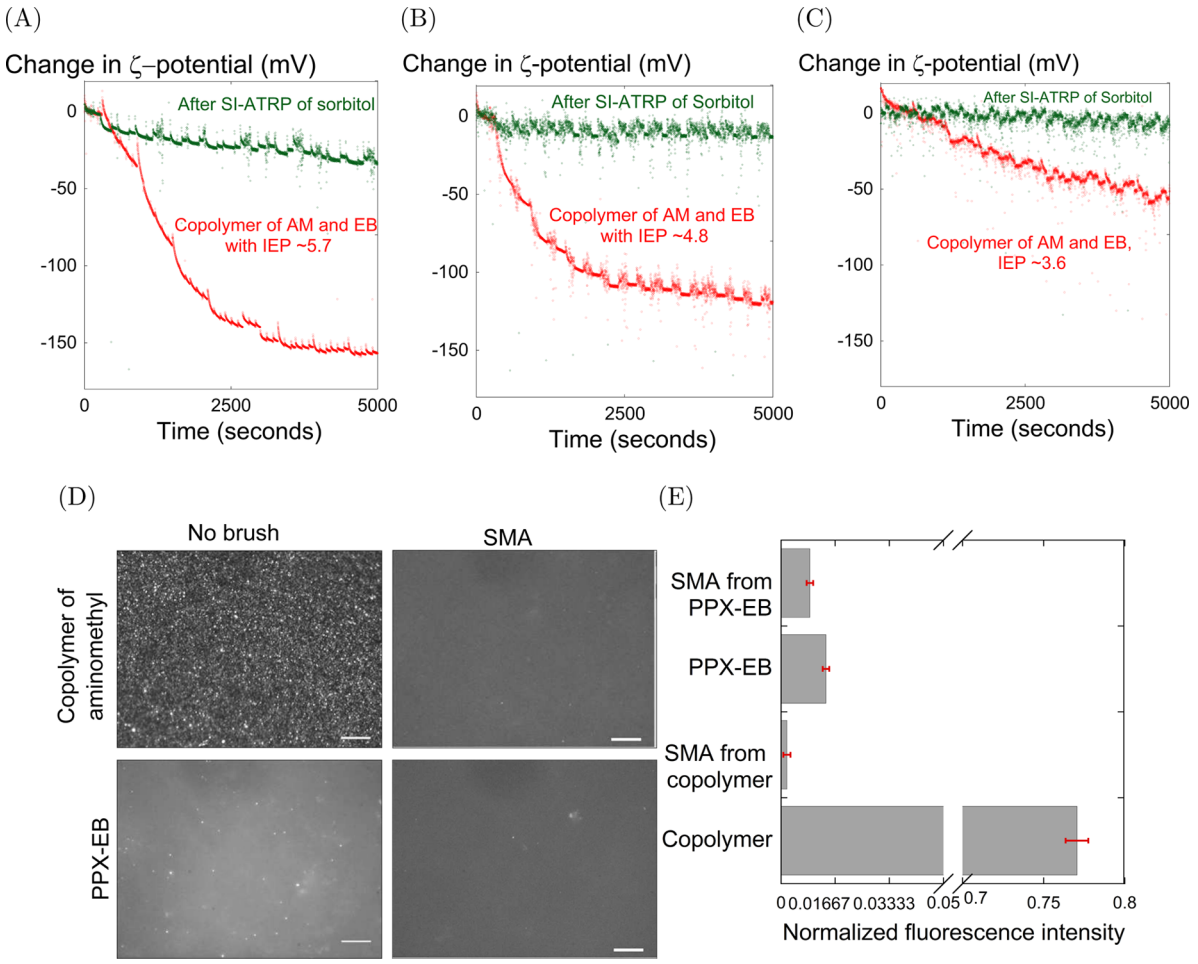

Figure 4. (A–C) Plots show how an increase in aminomethyl surface density (as measured by the isoelectric point) leads to a higher nanoparticle adsorption rate. The presence of the sorbitol brush is successful in retarding nanoparticle binding though in the case of (A), it is not entirely retarded. (D) Fluorescence study substantiates the results obtained from electrokinetic measurements. PS-COOH nanoparticles do not adhere to the sorbitol-grafted copolymer surfaces. Scale bar is 10 μm. (E) Comparison of surface density of fluorescent PS-COOH nanoparticles adsorbed on copolymer and PPX-EB before and after the SI-ATRP of sorbitol. High intensities were observed on the copolymer while low intensities were observed on PPX-EB (without amine groups) and also on sorbitol brushes grafted from PPX-EB and copolymer coatings. Error bars are in red.

sorbitol brushes were successful in preventing adsorption of PS-COOH nanoparticles almost completely. However, in the case of the copolymer with the highest density of amine groups (Figure 4A), the sorbitol brushes were able to reduce the rate and extent of adsorption but could not prevent it completely.

We studied the variation of sorbitol brush thicknesses with copolymer composition through ellipsometry, and these results are tabulated in Table S1. The thickness was greatest for the sorbitol brushes grafted from the copolymer with an IEP of 3.6 (8.7 nm) and lowest for the amine-rich copolymer with an IEP of 5.7 (3 nm). The copolymer with the intermediate IEP of 4.8 had 7.2 nm thick sorbitol brushes, which is the second largest brush thickness observed. This trend can be attributed to the lower density of ester bromide initiator groups in the more positively charged copolymer coatings, leading to a proportionally slower rate of brush growth and thinner brushes. Since initiator density and polymer brush growth rates have a linear relationship,[63] if we maintain identical SI-ATRP conditions, the copolymer bearing more EB groups would have thicker brushes than the copolymer with fewer EB groups.

Even though all the brush thickness values are within the Debye screening length (9.62 nm) of the ionic environment, they still succeed in retarding nanoparticle adsorption. It is possible that thicker brushes improve the resistance to adsorption as they carry higher thermodynamic costs of brush compression,[10] making it less likely for nanoparticles to adhere to the aminomethyl groups. However, this energy cost could be offset by promoting the electrostatic driving forces for adhesion in two ways: a higher AM surface density or a more acidic environment that leads to a greater degree of amine protonation. Therefore, the critical polymer brush thickness required to span the aminomethyl binding sites and prevent binding is dependent on the relative densities of initiator and aminomethyl groups and on the pH value of the medium. Future work will focus on the interplay between the degree of amine ionization and the chain length distribution of the sorbitol brushes and their roles in shaping nanoparticle adsorption. Our results so far suggest that we can not only modulate binding rates of the particles by changing the copolymer composition but also switch off binding by introducing sufficiently thick glycopolymer brushes.

To verify that sorbitol brushes function as barriers against nanoparticles and to validate the results from real-time electrokinetic measurements, we performed fluorescence microscopy to compare equilibrium adsorption of fluorescent nanoparticles. Four sets of surfaces were compared: the copolymer containing AM and EB with an IEP of 4.8 and

DOI: 10.1021/acs.langmuir.7b01553
Langmuir XXXX, XXX, XXX–XXX

PPX-EB without AM binding sites as well as the respective surfaces after grafting sorbitol brushes. We observed very little PS-COOH binding to the PPX-EB surfaces (no AM groups), both before and after the introduction of the sorbitol brushes, indicating that the AM groups are required for for the nanoparticle to bind. Interestingly, fluorescence measurements showed a high particle density on the copolymer surfaces and almost no particles on the sorbitol brushes grafted from the copolymer (Figure 4D,E). This observation is consistent with the decrease in ζ-potential observed during nanoparticle adsorption on the copolymers, and little or no change in ζ-potential during the study of nanoparticle adsorption on the sorbitol brush. ζ-potential has been a valuable tool to develop a temporal map of virus-like particle adsorption events transpiring on polymer brush interfaces that are populated with electrostatic tethers. This is the first ζ-potential based study that has studied adsorption kinetics of a biologically relevant adsorbate on a complex biomimetic interface. We suggest that this electrokinetic characterization approach, so far limited to simple homogeneous surfaces such as glass, quartz, and mica, can be readily extended to heterogeneous and nanotextured surfaces more typical of biomaterials.

CONCLUSIONS

Using real-time ζ-potential measurements, we were not only able to detect the well-known binding of neutravidin to biotinylated surfaces but also successfully quantify the neutravidin adsorption rate as a function of its concentration. By performing a parallel adsorption kinetics study using QCM, we could compare adsorption trends from ζ-potential with those obtained through QCM. Real-time ζ-potential measurements can be a powerful tool in understanding biomimetic surfaces possessing chemical heterogeneity, especially for applications sensitive to kinetic constraints as well as interfacial charge formation. We anticipate that this electrokinetic approach will be equally relevant to the study of affinity-based interactions of biological species with receptors as well as nonspecific binding events that are electrostatically driven.

Employing a combination of chemical vapor deposition copolymerization and surface-initiated atom transfer radical polymerization, we successfully multifunctional polymer coatings where the ratio of glycopolymer brushes and positively charged binding sites could be tuned. Because CVD copolymerization affords exquisite control over the surface composition and ultimately the surface charge of these coatings, the isoelectric point of the base copolymer can be increased simply by increasing the density of aminomethy functional groups. Increasing the aminomethyl surface concentration resulted in a progressively more rapid adsorption trajectory of the virus-like nanoparticles on the copolymer surface. In addition to tailoring the adsorption rates of nanoparticles by varying the copolymer composition, we can also reduce the adsorption extent to near-zero levels by growing sorbitol brushes from the initiator sites present on the copolymer.

We conclude that the adsorption of virus-like nanoparticles is shaped by the interplay of aminomethyl concentration and sorbitol brush architecture. In future work, we will investigate the effect of glycopolymer brush composition by developing coatings based on glucose, galactose, and mannose in their bioactive forms. We will also examine the adsorption of viruses such as adenoviruses and influenza on these surfaces as a function of amine density and glycopolymer brush architecture.

EXPERIMENTAL SECTION

The first and second sections describe chemical vapor deposition (CVD) polymerization and surface-initiated ATRP procedures. In the third, fourth, and fifth sections, characterization procedures for these coatings using ζ-potential, FTIR, and fluorescence are described. The sixth and seventh section explains the collection of real-time ζ-potential measurements using our electrokinetic analyzer and QCM measurements, respectively. Finally, the modeling procedure is summarized in the eighth section.

Chemical Vapor Deposition. As described in Nandivada et al.,[57] the precursor ethynyl[2,2]paracyclophane was sublimed at 100 °C and then subjected to thermal pyrolysis at 660 °C under low pressure (0.3 bar). The radical species that were generated thus adsorbed to the cooled substrate (15 °C) in the deposition chamber and underwent polymerization. Coatings composed of poly(4-ethynyl-*p*-xylylene-*co*-*p*-xylylene) (PPX-alkyne) were obtained. Poly(*p*-xylylene) (PPX-N) was prepared using the same procedure from [2,2]paracyclophane. 4-Aminomethyl[2,2]paracyclophane (PCP-AM) was obtained from Uniglobe Kisco, and coatings of poly(*p*-xylylene-4-aminomethyl)-*co*-(*p*-xylylene)] (PPX-AM) were prepared using the same operating parameters. To prepare poly[(*p*-xylylene-4-methyl-2-bromoisobutyrate)-*co*-(*p*-xylylene)] (PPX-EB), we employed the CVD conditions described in Jiang et al.[64] In brief, 32 mg of [2.2]-paracyclophane-4-methyl 2-bromoisobutyrate (PCP-EB) was sublimed at 115−125 °C under reduced pressure (0.3 mbar) and then pyrolyzed at 540 °C. Deposition of the polymer onto the substrate occurred on a sample holder maintained at 14 °C. To prepare a copolymer of [2.2]paracyclophane-4-methyl 2-bromoisobutyrate (PCP-EB) and 4-aminomethyl[2,2]paracyclophane (PCP-AM), a two-source CVD system was employed as described by Elkasabi et al.[65] An amount of 25 mg of PCP-AM was loaded into one source, and 32 mg of PCP-EB was loaded into the second source. The two source furnaces were heated independently to pyrolysis temperatures of 660 and 540 °C. The ratio of the two functional groups deposited on the target surface of the coating was controlled by changing the separation distance to the respective source. For the PCP-EB precursor, the separation was held constant at 0.8 cm, while for the PCP-AM, distances ranging from 2.8 to 3.2 cm were employed. Each precursor was sublimed between 80 and 110 °C at a pressure of 0.125 Torr. The sample holder was cooled to 14 °C and rotated continuously to ensure compositional homogeneity. At each source, a flow rate of 10 sccm was maintained using argon carrier gas in order to carry the sublimated dimers into the pyrolysis zone, from where they entered the deposition chamber to form coatings of poly[(*p*-xylylene-4-methyl-2-bromoisobutyrate)-*co*-(*p*-xylylene-4-aminomethyl)-*co*-(*p*-xylylene)] on the substrates. Once the PCP-EB precursor was sublimed completely, deposition was stopped immediately.

Glycopolymer Brush Synthesis. Sorbitol methacrylate monomer (SMA) was purchased from Monomer Polymer Dajac Laboratories, Trevose, PA, and polymerized from the PPX-EB initiator surfaces using SI-ATRP to yield glycopolymer brushes. Substrates bearing bromoisobutyryl groups (EB), either the homopolymer PPX-EB or the copolymer with PCP-AM, were prepared according to the CVD process described in previous sections. Prior to SI-ATRP, substrates were coated with either the copolymer or with PPX-EB. The initial and final values of the coating thickness were ascertained using nulling ellipsometry before and after SI-ATRP. Upon subtracting the initial thickness from the final thickness, the extent of brush growth could be measured. Results from ellipsometry studies are furnished in the Supporting Information. In a typical SI-ATRP run, copper(I) chloride, copper(II) chloride, and 2,2, bipyridyl were purchased from Sigma-Aldrich and used without further purification. Substrates were placed in a glovebag and degassed using three cycles of vacuum−argon purge and left at room temperature under argon. 8 mL of solution of 1 g/mL SMA in methanol, 2 mL of methanol, and 6 mL of water were mixed together in the monomer flask and then degassed by three cycles of freeze−pump−thaw. In parallel, a mixture of 3 mL of methanol and 1 mL of water was degassed using freeze−pump−thaw cycles in a separate catalyst flask. The catalyst was precomplexed with the ligand and dissolved separately from the monomer as the Cu^{I} and Cu^{II} tend to form a strong complex with the sorbitol monomer.

DOI: 10.1021/acs.langmuir.7b01553
Langmuir XXXX, XXX, XXX−XXX

After completion of the third freeze operation, 207.4 mg of bipyridyl, 35.5 mg of CuCl, and 7.9 mg of $CuCl_2$ were added to the catalyst flask under argon. Pump and thaw operations were continued subsequent to catalyst addition. Upon dissolution, the brown-colored catalyst mixture was added to the degassed monomer solution and mixed thoroughly at room temperature. This mixture was transferred to the glovebag and distributed such that each substrate was submerged completely in the reaction solution. The SI-ATRP reaction was allowed to proceed for 24 h under an argon atmosphere. Finally, substrates were rinsed repeatedly with 0.05 M EDTA solution and deionized water and dried.

FTIR Spectroscopy. To verify whether the desired functional groups were present on the surface of the polymer coatings, Fourier-transformed infrared (FTIR) spectroscopy was performed using Nicolet 6700 spectrophotometer in the grazing angle configuration against a gold background. Polymers were deposited on gold wafers, and 128 scans were collected with a resolution of 4 cm^{-1}. The FTIR spectra for the sorbitol brushes, PPX-alkyne, and PPX-EB are included in the Supporting Information.

Isoelectric Point Determination. For measuring the ζ-potential as a function of pH and to determine the isoelectric point (IEP), streaming current measurements were collected for multiple values of pH. Polymer coatings were prepared using the CVD processes described in previous sections. The clamping cell of the electrokinetic analyzer SurPASS (Anton Paar GmBH) was used in asymmetric mode[66] to acquire streaming current readings from the samples across a pH range of 3−6. Polypropylene foil was used as the reference. For each sample, titration was performed from the neutral to the acidic range using 0.1 M hydrochloric acid as the titrant and 0.001 M potassium chloride solution as the electrolyte. The pH value was controlled using an automated titration unit, which effected pH changes in increments of 0.3, while the electrolyte solution was stirred continuously. The electrolyte solution was purged continuously with nitrogen to prevent carbon dioxide dissolution and unintended changes in the pH value. Streaming current was measured using Ag/AgCl electrodes, and the Helmholtz−Smoluchwski equation[67−69] was applied to compute the ζ-potentials. Flow rates of 50−70 mL/min were observed at a pressure of 400 mbar, and a gap of 100−120 μm was maintained between the sample and the polypropylene reference standard. Samples were rinsed for 3 min before each measurement to equilibrate the surface against the electrolyte solution.

Fluorescence Measurements for Streptavidin and Nanoparticle Adsorption. Initially, samples were incubated in a solution of 0.1% (w/v) bovine serum albumin (Sigma-Aldrich) in phosphate buffered saline (PBS) for 30 min and then thoroughly rinsed with PBS. Subsequently, they were incubated in streptavidin-Cy3 (50 μg/mL) in PBS containing 0.02% (v/v) Tween 20 for 10 min. The substrate was then repeatedly washed with PBS and finally rinsed with deionized water. Substrates were dried and fluorescence micrographs recorded using a fluorescence scanner (Fluorochem M, Protein Simple Inc.) with an exposure time of 200 ms. The fluorescence intensity was extracted using ImageJ, and an average of readings obtained from three substrates for each sample group (PPX-N, PPX-alkyne clicked with PEG, PPX-alkyne clicked with biotin-PEG-azide[57]) was computed. The PS-COOH nanoparticles (Molecular Probes, carboxylated latex, 0.02 μm, 4% w/v) were purchased from Life Technologies and diluted down to a concentration of 8×10^{-7}g/mL in 0.1 mM phosphate buffer solution. The pH of the solution was adjusted to 5.90 by mixing NaH_2PO_4 and Na_2HPO_4 in the desired ratio. Glass coverslips coated with the polymers of interest were incubated with this nanoparticle suspension for 60 min and then imaged using a Nikon fluorescence microscope. ImageJ was used to quantify the density of adsorbed nanoparticles. Three substrates were used per sample group.

Adsorption Kinetics through ζ-Potential Measurements. This adsorption accessory (Attract, Anton-Paar GmbH) enabled the acquisition of ζ-potential values at a temporal resolution of 1 s. Since our samples were rigid and did not exhibit swelling, streaming current measurements accompanied by the Helmholtz−Smoluchowski correlation were used to compute ζ-potential. Measurements were performed in symmetric mode wherein both the top and bottom surfaces of the rectangular slit flow chamber were composed of the polymer coating of interest. Consistent with the procedure for IEP determination, a solution of 1 mM potassium chloride in Milli-Q water was continually purged with nitrogen gas to prevent the dissolution of carbon dioxide and subsequent changes in pH. Streaming current measurements were collected every second at a pressure of 200 mbar and a separation of 100−120 μm between the two parallel surfaces forming the flow chamber. Before the adsorbate species could be added, baseline measurements were acquired for a duration of 10 min to ascertain that a stable baseline was observed. After the baseline phase of the experiment was completed, the desired quantity of adsorbate was added, and the ζ-potential was recorded every second for the duration of the adsorption phase. The adsorption response was quantified by subtracting the average of ζ-potential values collected in the baseline phase from the ζ-potential observed at any instant of time. The magnitude of ζ-potential change was employed to determine the time and concentration dependence of adsorption. For adsorption kinetics experiments, carboxylated polystyrene nanoparticles (PS-COOH) were obtained from Thermo Fisher (Molecular Probes, carboxylated latex, 0.02 μm, 4% w/v). We employed a nanoparticle concentration of 8×10^{-7} g/mL. The pH value was maintained constant at 6.00 for the experiments investigating the effect of copolymer composition on nanoparticle adsorption.

For the neutravidin−biotin binding experiments, a 1 mM solution of phosphate buffer was employed. The buffer solution consisted of NaH_2PO_4 and Na_2HPO_4 mixed in a ratio of 81:19 v:v to achieve a pH of 7.4. The upper and lower faces of the rectangular slit chamber were coated with PPX-alkyne according to the procedure outlined in the second section. Substrates were subsequently biotinylated using biotin-PEG-azide (PG2-BNAZ-5k, Nanocs, NY) as described previously.[57] As a control, one pair of the PPX-alkyne coated surfaces was coated with 8-arm star PEG (MW 10K, PSB-881, Creative PEG works, NC) using 1 mg/mL of the functional PEG reagent, 1 mM $CuSO_4$ (Sigma-Aldrich), and 8 mM sodium ascorbate (Sigma-Aldrich). Neutravidin (catalog # 31050) was purchased from Life Technologies. To understand the effect of neutravidin concentration on binding kinetics, three concentration values were studied: 10, 100, and 1000 nM.

QCM Measurements To Measure the Binding Kinetics of Neutravidin to Biotin. The QCM-200 instrument (Stanford Research Systems, Sunnyvale, CA) was used for these studies. AT-cut quartz crystals coated with chrome/gold (O100RX1, Stanford Research Systems, Sunnyvale, CA) were functionalized with PPX-alkyne according to the procedure outlined in the second section. Quartz crystals were biotinylated using biotin-PEG-azide (PG2-BNAZ-5k, Nanocs, NY) as described previously.[57] As a control, one of the PPX-alkyne coated crystals was coated with 8-arm star PEG (MW 10K, PSB-881, Creative PEGWorks, Chapel Hill, NC) using 1 mg/mL of the PEG compound, 1 mM $CuSO_4$ (Sigma-Aldrich), and 8 mM sodium ascorbate (Sigma-Aldrich). Prior to measurement, the biotinylated crystal surfaces were allowed to equilibrate overnight in a 1 mM solution of phosphate buffer. The buffer solution consisted of NaH_2PO_4 and Na_2HPO_4 mixed in a ratio of 81:19 v:v to achieve a pH of 7.4. Then, they were mounted on a flow cell, and the phosphate buffer was pumped through the flow cell at a flow rate of 0.1 mL/h using a syringe pump. Once a stable baseline was observed, neutravidin was injected and the adsorption response recorded. The adsorbed neutravidin mass was computed from the frequency decrease through the Sauerbrey equation.[58]

Extraction of Apparent Rate Constants Using Kinetic Modeling. Neutravidin−biotin adsorption experiments performed with the electrokinetic analyzer, and the QCM yielded plots of adsorption response y as a function of time t. Assuming that the adsorption behavior conforms to a first-order kinetic model, these values were fitted according to the following monoexponential equation where A denotes plateau value of adsorption (units of mV for streaming potential and ng/cm^2 for QCM) and k is the apparent rate constant of adsorption with units of s^{-1}.

$$y = A(1 - e^{-kt})$$

The quality of the fit was assessed using the following model diagnostics: RMSE, which estimates total deviation of the response values from the fitted values; R-squared, which signifies how well the fit describes

DOI: 10.1021/acs.langmuir.7b01553
Langmuir XXXX, XXX, XXX−XXX

experimental behavior; and degree of freedom adjusted *R*-squared which detects "overfitting".

■ ASSOCIATED CONTENT

Supporting Information

The Supporting Information is available free of charge on the ACS Publications website at DOI: 10.1021/acs.langmuir.7b01553.

FTIR spectra, ellipsometric data, kinetic modeling, fluorescence, raw data from real-time ζ-potential measurements (PDF)

■ AUTHOR INFORMATION

Corresponding Author

*E-mail: lahann@umich.edu.

ORCID

Ramya Kumar: 0000-0002-8725-0023

Joerg Lahann: 0000-0002-3334-2053

Notes

The authors declare no competing financial interest.

■ ACKNOWLEDGMENTS

We acknowledge the Defense Threat Reduction Agency (DTRA) for funding provided through Grant HDTRA1-12-1-0039 as a part of the interfacial dynamics and reactivity program. We thank Vinod Ramachandran of Anton Paar GmbH for technical advice on the use of the electrokinetic analyzer.

■ REFERENCES

(1) Werner, C. In *Polymer Surfaces and Interfaces: Characterization, Modification and Applications*; Stamm, M., Ed.; Springer: Berlin, 2008; pp 299−318.

(2) Ratner, B. D. New ideas in biomaterials science-a path to engineered biomaterials. *J. Biomed. Mater. Res.* **1993**, *27*, 837−850.

(3) Hoffman, A. S. *Biomaterials: Interfacial Phenomena and Applications*; American Chemical Society: 1982; Chapter 2, pp 3−8.

(4) Shen, L.; Zhu, J. Heterogeneous surfaces to repel proteins. *Adv. Colloid Interface Sci.* **2016**, *228*, 40−54.

(5) Bedair, T. M.; Cho, Y.; Joung, Y. K.; Han, D. K. Biodegradable polymer brush as nanocoupled interface for improving the durability of polymer coating on metal surface. *Colloids Surf., B* **2014**, *122*, 808−817.

(6) Higaki, Y.; Kobayashi, M.; Murakami, D.; Takahara, A. Anti-fouling behavior of polymer brush immobilized surfaces. *Polym. J.* **2016**, *48*, 325−331.

(7) Hadjesfandiari, N.; Yu, K.; Mei, Y.; Kizhakkedathu, J. N. Polymer brush-based approaches for the development of infection-resistant surfaces. *J. Mater. Chem. B* **2014**, *2*, 4968−4978.

(8) Gon, S.; Bendersky, M.; Ross, J. L.; Santore, M. M. Manipulating Protein Adsorption using a Patchy Protein-Resistant Brush. *Langmuir* **2010**, *26*, 12147−12154.

(9) Gon, S.; Santore, M. M. Single Component and Selective Competitive Protein Adsorption in a Patchy Polymer Brush: Opposition between Steric Repulsions and Electrostatic Attractions. *Langmuir* **2011**, *27*, 1487−1493.

(10) Gon, S.; Kumar, K.-N.; Nüsslein, K.; Santore, M. M. How Bacteria Adhere to Brushy PEG Surfaces: Clinging to Flaws and Compressing the Brush. *Macromolecules* **2012**, *45*, 8373−8381.

(11) Kalasin, S.; Dabkowski, J.; Nüsslein, K.; Santore, M. M. The role of nano-scale heterogeneous electrostatic interactions in initial bacterial adhesion from flow: A case study with Staphylococcus aureus. *Colloids Surf., B* **2010**, *76*, 489−495.

(12) Duffadar, R. D.; Davis, J. M. Dynamic adhesion behavior of micrometer-scale particles flowing over patchy surfaces with nanoscale electrostatic heterogeneity. *J. Colloid Interface Sci.* **2008**, *326*, 18−27.

(13) Brittain, W. J.; Minko, S. A structural definition of polymer brushes. *J. Polym. Sci., Part A: Polym. Chem.* **2007**, *45*, 3505−3512.

(14) Qin, G.; Cai, C. Oxidative degradation of oligo(ethylene glycol)-terminated monolayers. *Chem. Commun.* **2009**, 5112−5114.

(15) Chen, S.; Li, L.; Zhao, C.; Zheng, J. Surface hydration: Principles and applications toward low-fouling/nonfouling biomaterials. *Polymer* **2010**, *51*, 5283−5293.

(16) Luk, Y.-Y.; Kato, M.; Mrksich, M. Self-Assembled Monolayers of Alkanethiolates Presenting Mannitol Groups Are Inert to Protein Adsorption and Cell Attachment. *Langmuir* **2000**, *16*, 9604−9608.

(17) Reitsma, S.; Slaaf, D. W.; Vink, H.; van Zandvoort, M. A. M. J.; oude Egbrink, M. G. A. The endothelial glycocalyx: composition, functions, and visualization. *Pfluegers Arch.* **2007**, *454*, 345−359.

(18) Ham, H. O.; Park, S. H.; Kurutz, J. W.; Szleifer, I. G.; Messersmith, P. B. Antifouling Glycocalyx-Mimetic Peptoids. *J. Am. Chem. Soc.* **2013**, *135*, 13015−13022.

(19) Hower, J. C.; He, Y.; Bernards, M. T.; Jiang, S. Understanding the nonfouling mechanism of surfaces through molecular simulations of sugar-based self-assembled monolayers. *J. Chem. Phys.* **2006**, *125*, 214704.

(20) Hower, J. C.; He, Y.; Jiang, S. A molecular simulation study of methylated and hydroxyl sugar-based self-assembled monolayers: Surface hydration and resistance to protein adsorption. *J. Chem. Phys.* **2008**, *129*, 215101.

(21) Michen, B.; Graule, T. Isoelectric points of viruses. *J. Appl. Microbiol.* **2010**, *109*, 388−397.

(22) Young, A. G.; McQuillan, A. J. Adsorption/Desorption Kinetics from ATR-IR Spectroscopy. Aqueous Oxalic Acid on Anatase TiO_2. *Langmuir* **2009**, *25*, 3538−3548.

(23) Cuba-Chiem, L. T.; Huynh, L.; Ralston, J.; Beattie, D. A. In Situ Particle Film ATR FTIR Spectroscopy of Carboxymethyl Cellulose Adsorption on Talc: Binding Mechanism, pH Effects, and Adsorption Kinetics. *Langmuir* **2008**, *24*, 8036−8044.

(24) Seitz, R.; Brings, R.; Geiger, R. Protein adsorption on solid-liquid interfaces monitored by laser-ellipsometry. *Appl. Surf. Sci.* **2005**, *252*, 154−157.

(25) Vörös, J.; Ramsden, J. J.; Csúcs, G.; Szendro, I.; De Paul, S. M.; Textor, M.; Spencer, N. D. Optical grating coupler biosensors. *Biomaterials* **2002**, *23*, 3699−3710.

(26) Höök, F.; Vörös, J.; Rodahl, M.; Kurrat, R.; Böni, P.; Ramsden, J. J.; Textor, M.; Spencer, N. D.; Tengvall, P.; Gold, J.; Kasemo, B. A comparative study of protein adsorption on titanium oxide surfaces using in situ ellipsometry, optical waveguide lightmode spectroscopy, and quartz crystal microbalance/dissipation. *Colloids Surf., B* **2002**, *24*, 155−170.

(27) Wertz, C. F.; Santore, M. M. Adsorption and Reorientation Kinetics of Lysozyme on Hydrophobic Surfaces. *Langmuir* **2002**, *18*, 1190−1199.

(28) Toscano, A.; Santore, M. M. Fibrinogen Adsorption on Three Silica-Based Surfaces: Conformation and Kinetics. *Langmuir* **2006**, *22*, 2588−2597.

(29) Schönherr, H.; Johnson, J. M.; Lenz, P.; Frank, C. W.; Boxer, S. G. Vesicle Adsorption and Lipid Bilayer Formation on Glass Studied by Atomic Force Microscopy. *Langmuir* **2004**, *20*, 11600−11606.

(30) Cheng, C. I.; Chang, Y.-P.; Chu, Y.-H. Biomolecular interactions and tools for their recognition: focus on the quartz crystal microbalance and its diverse surface chemistries and applications. *Chem. Soc. Rev.* **2012**, *41*, 1947−1971.

(31) Dixon, M. C. Quartz Crystal Microbalance with Dissipation Monitoring: Enabling Real-Time Characterization of Biological Materials and Their Interactions. 2008, 151−158.

(32) Mao, Y.; Bao, Y.; Wang, W.; Li, Z.; Li, F.; Niu, L. Development and Application of Time-Resolved Surface Plasmon Resonance Spectrometer. *Am. J. Anal. Chem.* **2011**, *2*, 589−604.

(33) Wang, W.; Wolff, M. W.; Reichl, U.; Sundmacher, K. Avidity of influenza virus: Model-based identification of adsorption kinetics from surface plasmon resonance experiments. *Journal of Chromatography A* **2014**, *1326*, 125−129.

DOI: 10.1021/acs.langmuir.7b01553
Langmuir XXXX, XXX, XXX−XXX

(34) Scherr, S. M.; Daaboul, G. G.; Trueb, J.; Sevenler, D.; Fawcett, H.; Goldberg, B.; Connor, J. H.; Ünlü, M. S. Real-time monitroing of Individual Viruses in Complex Media. *ACS Nano* **2016**, *10*, 2827.
(35) Tandon, V.; Bhagavatula, S. K.; Nelson, W. C.; Kirby, B. J. Zeta potential and electroosmotic mobility in microfluidic devices fabricated from hydrophobic polymers: 1. The origins of charge. *Electrophoresis* **2008**, *29*, 1092−1101.
(36) Guo, K.; Freguia, S.; Dennis, P. G.; Chen, X.; Donose, B. C.; Keller, J.; Gooding, J. J.; Rabaey, K. Effects of Surface Charge and Hydrophobicity on Anodic Biofilm Formation, Community Composition, and Current Generation in Bioelectrochemical Systems. *Environ. Sci. Technol.* **2013**, *47*, 7563−7570.
(37) Patolsky, F.; Zheng, G.; Hayden, O.; Lakadamyali, M.; Zhuang, X.; Lieber, C. M. Electrical detection of single viruses. *Proc. Natl. Acad. Sci. U. S. A.* **2004**, *101*, 14017−14022.
(38) Froeter, P.; Huang, Y.; Cangellaris, O. V.; Huang, W.; Dent, E. W.; Gillette, M. U.; Williams, J. C.; Li, X. Toward Intelligent Synthetic Neural Circuits: Directing and Accelerating Neuron Cell Growth by Self-Rolled-Up Silicon Nitride Microtube Array. *ACS Nano* **2014**, *8*, 11108−11117.
(39) Tofail, S. A. M.; Bauer, J. Electrically Polarized Biomaterials. *Adv. Mater.* **2016**, *28*, 5470−5484.
(40) Hunt, J. A.; Flanagan, B. F.; McLaughlin, P. J.; Strickland, I.; Williams, D. F. Effect of biomaterial surface charge on the inflammatory reponse: Evaluation of cellular infiltration and TNFα production. *J. Biomed. Mater. Res.* **1996**, *31*, 139−144.
(41) Norde, W.; Fraaye, J. G. Î. M.; Lyklema, J. Protein Adsorption at Solid-Liquid Interfaces: A Colloid-Chemical Approach. 1987.
(42) Norde, W.; Rouwendal, E. Streaming potential measurements as a tool to study protein adsorption kinetics. *J. Colloid Interface Sci.* **1990**, *139*, 169−176.
(43) Etheve, J.; Dejardin, P. Adsorption Kinetics of Lysozyme on Silica at pH 7. 4: Correlation between Streaming Potential and Adsorbed Amount. *Langmuir* **2002**, *18*, 1777−1785.
(44) Rezwan, K.; Meier, L. P.; Rezwan, M.; Vörös, J.; Textor, M.; Gauckler, L. J. Bovine Serum Albumin Adsorption onto Colloidal Al_2O_3 Particles: A New Model Based on Zeta Potential and UV - Vis Measurements. *Langmuir* **2004**, *20*, 10055−10061.
(45) Wasilewska, M.; Adamczyk, Z. Fibrinogen Adsorption on Mica Studied by AFM and in Situ Streaming Potential Measurements. *Langmuir* **2011**, *27*, 686−696.
(46) Armanious, A.; Aeppli, M.; Jacak, R.; Refardt, D.; Sigstam, T.; Kohn, T.; Sander, M. Viruses at Solid-Water Interfaces: A Systematic Assessment of Interactions Driving Adsorption. *Environ. Sci. Technol.* **2016**, *50*, 732−743.
(47) Gutierrez, L.; Mylon, S. E.; Nash, B.; Nguyen, T. H. Deposition and Aggregation Kinetics of Rotavirus in Divalent Cation Solutions. *Environ. Sci. Technol.* **2010**, *44*, 4552−4557.
(48) Adamczyk, Z.; Zaucha, M.; Zembala, M. Zeta Potential of Mica Covered by Colloid Particles: A Streaming Potential Study. *Langmuir* **2010**, *26*, 9368−9377.
(49) Savaji, K. V.; Niitsoo, O.; Couzis, A. Journal of Colloid and Interface Science Influence of particle/solid surface zeta potential on particle adsorption kinetics. *J. Colloid Interface Sci.* **2014**, *431*, 165−175.
(50) Dev, A.; Horak, J.; Kaiser, A.; Yuan, X.; Perols, A.; Björk, P.; Karlström, A. E.; Kleimann, P.; Linnros, J. Electrokinetic effect for molecular recognition: A label-free approach for real-time biosensing. *Biosens. Bioelectron.* **2016**, *82*, 55−63.
(51) Jain, A.; Cheng, K. The principles and applications of avidin-based nanoparticles in drug delivery and diagnosis. *J. Controlled Release* **2017**, *245*, 27−40.
(52) Srisa-Art, M.; Dyson, E. C.; deMello, A. J.; Edel, J. B. Monitoring of Real-Time Streptavidin-Biotin Binding Kinetics Using Droplet Microfluidics. *Anal. Chem.* **2008**, *80*, 7063−7067.
(53) Livnah, O.; Bayer, E. A.; Wilchek, M.; Sussman, J. L. Three-dimensional structures of avidin and the avidin-biotin complex. *Proc. Natl. Acad. Sci. U. S. A.* **1993**, *90*, 5076−5080.
(54) Su, X.; Wu, Y.-j.; Knoll, W. Comparison of surface plasmon resonance spectroscopy and quartz crystal microbalance techniques for studying DNA assembly and hybridization. *Biosens. Bioelectron.* **2005**, *21*, 719−726.
(55) Seto, H.; Yamashita, C.; Kamba, S.; Kondo, T.; Hasegawa, M.; Matsuno, M.; Ogawa, Y.; Hoshino, Y.; Miura, Y. Biotinylation of Silicon and Nickel Surfaces and Detection of Streptavidin as Biosensor. *Langmuir* **2013**, *29*, 9457−9463.
(56) Nguyen, T. T.; Sly, K. L.; Conboy, J. C. Comparison of the Energetics of Avidin, Streptavidin, NeutrAvidin, and Anti-Biotin Antibody Binding to Biotinylated Lipid Bilayer Examined by Second-Harmonic Generation. *Anal. Chem.* **2012**, *84*, 201−208.
(57) Nandivada, H.; Chen, H.-y.; Bondarenko, L.; Lahann, J. Reactive Polymer Coatings that "Click. *Angew. Chem., Int. Ed.* **2006**, *45*, 3360−3363.
(58) Sauerbrey, G. Verwendung von Schwingquarzen zur Wägung dünner Schichten und zur Mikrowägung. *Eur. Phys. J. A* **1959**, *155*, 206−222.
(59) Edwards, P.; Gill, A.; Pollardknight, D.; Hoare, M.; Buckle, P.; Lowe, P.; Leatherbarrow, R. Kinetics of Protein-Protein Interactions at the Surface of an Optical Biosensor. *Anal. Biochem.* **1995**, *231*, 210−217.
(60) Zhang, L.; Huo, W.; Gao, Y.; Shi, S.; Gao, Y. Determination of Affinity and Kinetic Constants of the Biotin-Streptavidin Complex Using Microfluidic GMR Biosensors. *IEEE Trans. Magn.* **2015**, *51*, 1−4.
(61) Weinbaum, S.; Zhang, X.; Han, Y.; Vink, H.; Cowin, S. C. Mechanotransduction and flow across the endothelial glycocalyx. *Proc. Natl. Acad. Sci. U. S. A.* **2003**, *100*, 7988−7995.
(62) Koopal, L. K.; Avena, M. A simple model for adsorption kinetics at charged solid-liquid interfaces A simple model for adsorption kinetics at charged solid-liquid interfaces. *Colloids Surf., A* **2001**, *192*, 93−107.
(63) Jones, D. M.; Brown, A. A.; Huck, W. T. S. Surface-Initiated Polymerizations in Aqueous Media-Effect of Initiator Density. *Langmuir* **2002**, *18*, 1265−1269.
(64) Jiang, X.; Chen, H.-Y.; Galvan, G.; Yoshida, M.; Lahann, J. Vapor-Based Initiator Coatings for Atom Transfer Radical Polymerization. *Adv. Funct. Mater.* **2008**, *18*, 27−35.
(65) Elkasabi, Y.; Chen, H.-Y.; Lahann, J. Multipotent Polymer Coatings Based on Chemical Vapor Deposition Copolymerization. *Adv. Mater.* **2006**, *18*, 1521−1526.
(66) Walker, S. L.; Bhattacharjee, S.; Hoek, E. M. V.; Elimelech, M. A Novel Asymmetric Clamping Cell for Measuring Streaming Potential of Flat Surfaces. *Langmuir* **2002**, *18*, 2193−2198.
(67) Werner, C.; Zimmermann, R.; Kratzmüller, T. Streaming potential and streaming current measurements at planar solid/liquid interfaces for simultaneous determination of zeta potential and surface conductivity. *Colloids Surf., A* **2001**, *192*, 205−213.
(68) Werner, C.; Körber, H.; Zimmermann, R.; Dukhin, S.; Jacobasch, H.-J. Extended Electrokinetic Characterization of Flat Solid Surfaces. *J. Colloid Interface Sci.* **1998**, *208*, 329−346.
(69) Lyklema, J.; Overbeek, J. On the interpretation of electrokinetic potentials. *J. Colloid Sci.* **1961**, *16*, 501−512.

DOI: 10.1021/acs.langmuir.7b01553
Langmuir XXXX, XXX, XXX−XXX